

Band structure of compensated *n-i-p-i* superlattices

H. Yan and H. X. Jiang*

Center for Fundamental Materials Research and Department of Physics and Astronomy, Michigan State University, East Lansing, Michigan 48824-1116

(Received 10 September 1987)

The band structure of compensated *n-i-p-i* doping superlattices has been investigated for the first time by using the multistep-potential approach as the real potential form and by using numerical calculations. The dispersion of compensated *n-i-p-i* superlattices is shown to be stronger than that of compositional superlattices. The first three allowed conduction minibands and forbidden minigaps as functions of period length *L* are presented.

In recent years there has been great interest in both theoretical and experimental studies of doping superlattices.^{1,2} The *n-i-p-i* doping superlattices are systems composed of a periodic sequence of ultrathin *n*- and *p*-type doped layers with intrinsic layers in between.³⁻⁶ In addition to the properties of the compositional superlattices, doping superlattices, however, show a number of novel properties related to the electrostatic origin of the superlattice potential. The lowest electron and the uppermost hole subband states are locally separated from each other. The effective energy gap as well as the electron and hole concentration can be varied arbitrarily over a wide range in *n-i-p-i* superlattices either optically or by carrier injection into the bulk. These unique features open a new field for both basic research and device application.

Although *n-i-p-i* superlattices have been discovered for a few years, many important physical properties are still unknown because of their complicated structures. To our knowledge, the most important properties—the dispersion, miniband structure, and, consequently, the effective energy gap of *n-i-p-i* superlattices—have never been carefully investigated previously. One usually uses an uncoupled quantum well to estimate the energy levels. By the approximation of an infinitely deep quantum well, the harmonical-oscillator-type energy levels have been widely used,⁷⁻⁹ which can be written as

$$E_\nu = (\nu + \frac{1}{2})\hbar\omega, \quad \nu = 0, 1, 2, \dots \tag{1}$$

where $\omega = (4\pi n_D e^2 / m_e \epsilon)^{1/2}$, and m_e and ϵ are the electron effective mass and dielectric constant, respectively. It is obvious that this approximation is not valid in many cases. First, when the period length is small, the infinite potential well is much too strong compared with the real potential, which is finite and periodic. Secondly, there is no dispersion in energies for electrons and holes under this approximation. As we know, the dispersion in energies for electrons and holes in a periodic potential always exists.

In this paper, by using the multistep-potential approach proposed by Ando and Itoh¹⁰ as the real potential, we calculate numerically the band structure of compensated *n-i-p-i* superlattices. The first three allowed conduction minibands and forbidden minigaps as functions of period length *L* are presented. For comparison, we also calculated the band structure of *n*- and *p*-type doped superlattices without intrinsic layers in between ($d_i = 0$, *n-p* superlattices).

The potential form for a compensated *n-i-p-i* superlattice ($n_D d_n = n_A d_p$),⁶ as shown in Fig. 1, can be written as

$$V(x) = V_0(x - mL), \quad -L/2 < x - mL \leq L/2 \tag{2}$$

with *m* being integers ($m = 0, \pm 1, \pm 2, \dots$) and *x* being the coordinate in the doping direction, and

$$V_0(x) = (2\pi e^2 / \epsilon) \times \begin{cases} \{n_A(d_p^2/4 - |x|^2) + n_D d_n(d_n/4 + d_i)\}, & |x| \leq d_p/2 & (3a) \\ \{n_A d_p(d_p/2 - |x|) + n_D d_n(d_n/4 + d_i)\}, & d_p/2 < |x| \leq d_p/2 + d_i & (3b) \\ n_D(|x| - L/2)^2, & d_p/2 + d_i < |x| \leq L/2. & (3c) \end{cases}$$

Here d_n , d_p , and d_i are the width of *n*-type doped, *p*-type doped, and intrinsic layer materials, respectively. n_D and n_A are the *n*- and *p*-layer doping concentrations. $L = d_n + d_p + 2d_i$ is the period length.

Using the transfer-matrix method,^{11,12} and the continuity conditions of wave functions and their derivative across the interfaces, we can obtain the dispersion relation from the following equation:

$$\cos(qL) = \frac{1}{2} \text{Tr}(M), \tag{4}$$

where *M* is the transfer matrix which connects the constant coefficients in the solution of the Schrödinger equation in the *n*th period to those in the (*n* - 1)th period and *q* is the wave vector. By using the multistep-potential approach¹⁰ with 200 steps in each period as the real potential, we can easily obtain an expression for the matrix *M*. The dispersion relation has been numerically evaluated from the expression of *M*. In this paper, the calculations are performed for the compensated *n-i-p-i* GaAs superlattices. The dielectric constant ϵ and electron effective

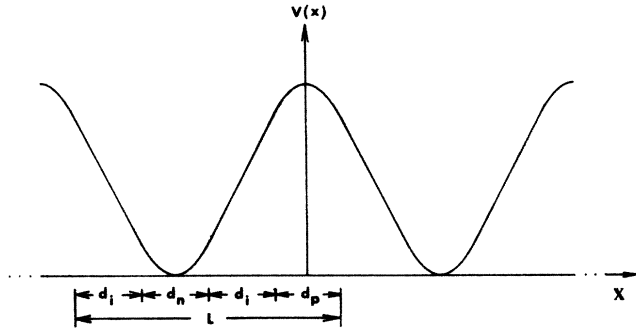


FIG. 1. Band profile of the compensated *n-i-p-i* semiconductor superlattice with $d_i=d_p=d_n=L/4$, and L is the period length.

mass m_e are 12.5 and $0.067m_0$, respectively,^{13,14} where m_0 is the electron mass in free space.

Figure 2 shows the dispersion of conduction minibands with $n_D=n_A=10^{18}/\text{cm}^3$, $d_i=d_p=d_n=L/4$, (a) $L=120 \text{ \AA}$, and (b) $L=400 \text{ \AA}$. The dashed lines represent the energy levels of E_ν in Eq. (1). In Fig. 2(a) we have $\nu=0$ and 1, and in Fig. 2(b) we have $\nu=0, 1$, and 2. From Fig. 2(a) we can see that when the period length L is small, the dispersion in energy is very large even for the lowest sub-

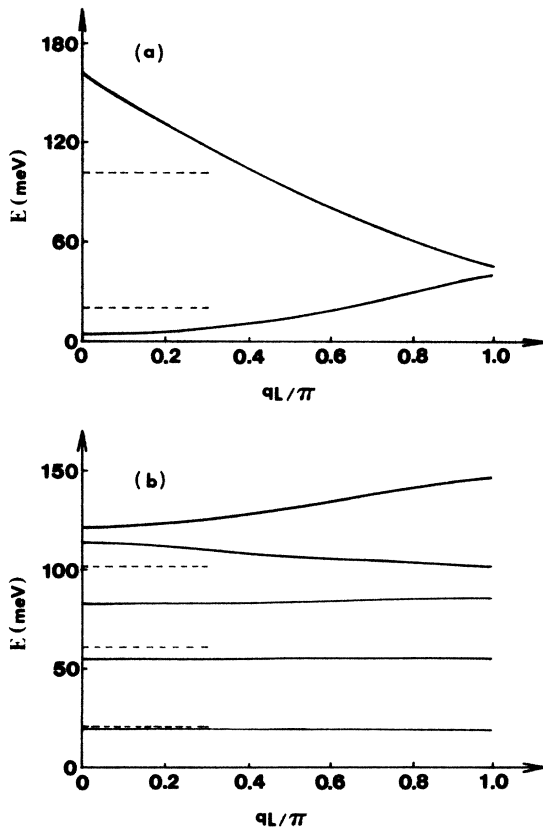


FIG. 2. Dispersion of conduction bands with $n_D=n_A=10^{18}/\text{cm}^3$, $d_i=d_p=d_n=L/4$, and (a) $L=120 \text{ \AA}$, (b) $L=400 \text{ \AA}$. Dashed lines are the energy levels of $E_\nu=(\nu+\frac{1}{2})\hbar\omega$ with $\nu=0$ and 1 for (a) and $\nu=0, 1$, and 2 for (b).

bands ($n=1$ and 2). The energy levels E_ν lie between the energies at the center of band and edge of band. The ground-state energy is about 16 meV below $\frac{1}{2}\hbar\omega$. Compared with GaAs-Ga_{1-x}Al_xAs compositional superlattice of the same periodic length $L=120 \text{ \AA}$ and $x\sim 0.3$, the dispersion of the *n-i-p-i* superlattice is much stronger than that of the compositional superlattice.¹² As we know for the compositional superlattice, the dispersion of the *n-i-p-i* superlattices is also larger for higher subbands. For the large period length $L(=400 \text{ \AA})$, Fig. 2(b) shows that the dispersions for the three lowest subbands ($n=1, 2$, and 3) are very small. The subbands are always located below the corresponding energy levels of E_ν . The differences between the subband energies and E_ν are smallest for the lowest subbands and increase for higher subbands. From Fig. 2 we can see that even for the *n-i-p-i* superlattice with relatively large period length, the expression of $E_\nu=(\nu+\frac{1}{2})\hbar\omega$ for the energy levels is not a good approximation for higher subbands, thus pointing out the importance of the present calculations.

Figure 3 shows the first three allowed conduction minibands (shaded area) and minigaps as functions of period length L with $n_D=n_A=10^{18}/\text{cm}^3$ and $d_i=d_p=d_n=L/4$. The dashed lines are the energy levels of E_ν with $\nu=0, 1$, and 2. Note that the energy is measured from the bottom of the potential well and this position varies for different L . The advantage in presenting the results in this way is that the energy levels corresponding to the infinitely deep quantum well, E_ν , are straight lines in the figure. This al-

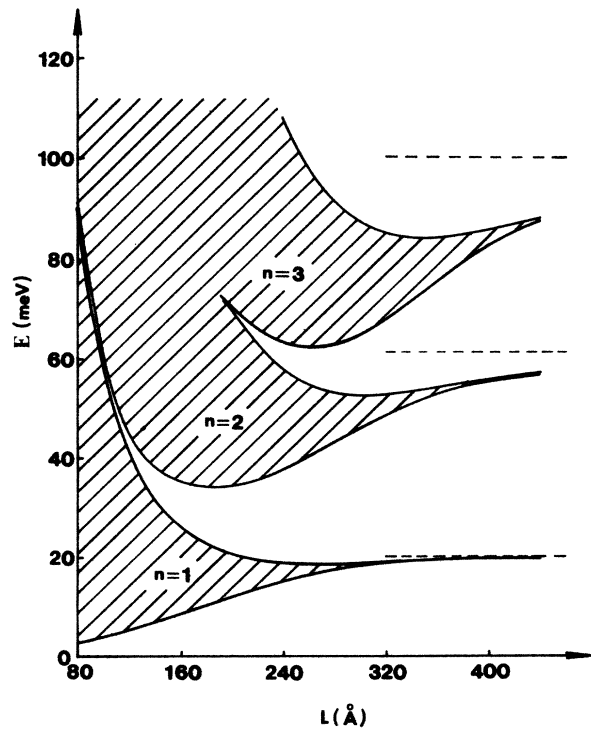


FIG. 3. The first three allowed conduction minibands (shaded area) and minigaps as functions of period length L with $n_D=n_A=10^{18}/\text{cm}^3$, $d_i=d_p=d_n=L/4$, and $L=400 \text{ \AA}$. Dashed lines are the energy levels of $E_\nu=(\nu+\frac{1}{2})\hbar\omega$ with $\nu=0, 1$, and 2.

TABLE I. Energy of the electron (meV) at $kL=0$ and $kL=\pi$ of the first five minibands for *n-i-p-i* and *n-p* superlattices with $L=400$ Å and $n_D=n_A=10^{18}/\text{cm}^3$.

Subband	<i>n-p</i> ($d_i=0$)		<i>n-i-p-i</i> ($d_i=L/4$)	
	$kL=0$	$kL=\pi$	$kL=0$	$kL=\pi$
$n=1$	20.2915	20.2926	19.4714	19.4775
$n=2$	60.5693	60.5344	55.2661	55.0379
$n=3$	98.620	99.309	82.646	85.145
$n=4$	134.593	128.795	113.596	102.597
$n=5$	148.39	167.94	121.20	145.79

lows us to make a comparison easily. A few important results can be obtained from Fig. 3. First, when the period length L is large, the band levels approach the energy levels of E_v and the widths of the subbands approach zero, as they should. Second, the ground-state energy monotonically decreases as L decreases. The fast decrease starts at about $L=320$ Å. The widths of the subbands increase and the minigaps decrease as L decreases. Third, except for the ground state, energies at the center of band and edge of band, have minima at different period length L . This behavior can be understood by realizing that the energies at the center of band and edge of band depend on the period length L and potential height V_0 , while V_0 here is related to L . As L increases, the well width increases, thus decreasing the energy levels. Meanwhile, potential height increases as a result of increasing L , and this increases the energy level. The dependence of energy levels on L is determined by these two competitive factors. The dependence of the energy level at E_0 on L can be written as

$$\frac{dE}{dL} \Big|_{E=E_0} = \left(\frac{\partial E}{\partial L} + \frac{\partial E}{\partial V_0} \frac{\partial V_0}{\partial L} \right) \Big|_{E=E_0}$$

and we note that these two terms have the opposite signs. The minima in Fig. 3 correspond to the positions of energy E_0 with $dE/dL|_{E=E_0}=0$. For the ground state, because the energy level lies very close to the bottom of the well, the second term is dominated and so the energy monotonically decreases as L decreases. Fourth, at about $L=180$ Å, $n=2$ and $n=3$ subbands overlap each other. The same behavior occurred at about $L=80$ Å for $n=1$ and 2 subbands. We can write the number of subbands, N , as a function of L as

$$N(L) = 1 + \sum_i \Theta(L - L_i), \quad (5)$$

where $\Theta(x)$ is a step function which equals 1 if $x > 0$ and

0 otherwise. L_i is about 80 and 180 Å for $i=1$ and 2, respectively.

To see the effects of the intrinsic layers, we also calculated the band structure of *n-p* superlattice with $d_n=d_p=L/2$. The results for the *n-i-p-i* and *n-p* superlattices are listed in Table I. From Table I we can see that the intrinsic layers decrease the energy levels. For $L=400$ Å and $n_D=n_A=10^{18}/\text{cm}^3$, there is about an 0.8-meV shift at $kL=0$ and $kL=\pi$ for the $n=1$ subband. This shift increases as n increases. For $n=5$, the shifts are 27.19 meV at $kL=0$ and 22.15 meV at $kL=\pi$. Also, the dispersion is larger for the *n-i-p-i* superlattice than for the *n-p* superlattice, so the *n-i-p-i* superlattices have a relatively weaker confinement to electrons and holes compared with *n-p* superlattices. This can be understood because the potential height of the *n-p* superlattice is higher than that of the *n-i-p-i* superlattice.

In conclusion, we have calculated the dispersion in energies and miniband structures of compensated doping superlattices. The method used here is simple, but effectively gives very accurate results. The results obtained here were compared with energy levels of $E_v=(v+\frac{1}{2})\hbar\omega$, which shows that E_v is not a good approximation in many cases. The first three allowed minibands and minigaps as functions of period length L were presented. The effects of intrinsic layers to the band structure were also investigated. These results are important both in the basic research and device applications. The detailed calculations and the band structures for different doping concentrations, and the effective energy gap of the heavy and light holes as functions of period length and doping concentrations, will be presented in a forthcoming paper.

ACKNOWLEDGMENT

We are grateful to J. Y. Lin for a critical reading of, and comments on, the manuscript.

*To whom all correspondence should be addressed.

¹K. Ploog and G. H. Döhler, Adv. Phys. **32**, 285 (1983).

²G. H. Döhler, Phys. Scr. **24**, 430 (1981).

³G. H. Döhler, Phys. Status Solidi B **52**, 79 (1972); **52**, 533 (1972).

⁴K. Ploog, A. Fischer, G. H. Döhler, and H. Kunzel, in *Gallium Arsenide and Related Compounds, 1980*, IOP Conf. Ser. No. 56, edited by H. W. Thim (Institute of Physics, London, 1981), p. 721.

⁵G. H. Döhler, H. Kunzel, D. Olego, K. Ploog, P. Ruden, H. J. Stolz, and G. Abstreiter, Phys. Rev. Lett. **47**, 864 (1981).

⁶G. H. Döhler, J. Vac. Sci. Technol. **16**, 851 (1979).

⁷G. H. Döhler, J. Vac. Sci. Technol. B **1**, 278 (1983).

⁸K. Ploog, in *Two-Dimensional Systems, Heterostructures, and Superlattices*, edited by G. Bauer, F. Kuchar, and H. Heinrich (Springer-Verlag, Berlin, 1984), p. 220.

⁹M. Gal, J. M. Viner, and P. C. Taylor, J. Vac. Sci. Technol. **5**, 504 (1987).

¹⁰Y. Ando and T. Itoh, *J. Appl. Phys.* **61**, 1497 (1987).

¹¹E. Merzbacher, *Quantum Mechanics*, 2nd ed. (Wiley, New York, 1970), pp. 73–105.

¹²H. X. Jiang and J. Y. Lin, *J. Appl. Phys.* **61**, 624 (1987).

¹³R. L. Greene and K. K. Bajaj, *Phys. Rev. B* **31**, 913 (1984).

¹⁴*Numerical Data and Functional Relationship in Science and Technology*, Vol. 17 of *Landolt-Börnstein*, new series, edited by O. Madelung (Springer, Berlin, 1982).